Microstructure analysis and biological properties of sodium hydroxyapatite with added citric acid to electrolyte

Y. H. Lei [a], J. H. Hai [a,*], C. L Shan [b], X. Z. Zhang [a], L. Jing [a], X. H. Ma [c]
[a] *College of Mechanical Engineering, Xinjiang University, Urumqi 830046, Xinjiang Uygur Autonomous Region, China*
[b] *The Sixth Affiliated Hospital of Xinjiang Medical University, Urumqi 830054, Xinjiang Uygur Autonomous Region, China*
[c] *Xin Jiang Key Laboratory of Mental Development and Learning Science, College of Psychology, Xinjiang Normal University, Urumqi, Xinjiang, 830017, China*

The growth orientation of the HA crystals was controlled through the addition of sodium citrate to the electrolyte during electrochemical deposition. Additionally, the impact of the sodium citrate inhibition time on the morphology of HA crystals across various deposition periods was evaluated. The differences in biocompatibility of coatings due to the addition of sodium citrate were elucidated. The coatings were characterized through scanning electron microscopy, X-ray diffraction, and Fourier-transform infrared spectroscopy. The results revealed that controlling the crystal-oriented growth of HA significantly influenced cell adhesion and migration. This enhancement improved the suitability of the porous Ti scaffold for biomedical implant applications.

(Received October 29, 2024; Accepted March 20, 2025)

Keywords: TiO_2 nanotubes, Hydroxyapatite, Mechanical binding strength, Bioactivity, Composite coating

1. Introduction

Advancements in additive manufacturing have enabled the production of complex structures for personalized implants. These implants are designed with pore shapes that match the size and shape of damaged bone tissues, leading to enhanced cell adhesion and material transport compared with conventional implants. Selective laser melting is a precise and cost-effective technique for fabricating titanium (Ti)-based implants[1]. Ti and its alloys are widely utilized as orthopedic biomaterials owing to their suitable mechanical strength, favorable modulus of elasticity, biocompatibility with bone tissue, and low toxicity[2]. However, Ti exhibits low bioactivity and lacks osteoconductivity, which can lead to prolonged recovery times after surgery. To address these issues, numerous studies have explored the use of bioactive materials to promote interactions between implants and host tissues, thereby achieving bone tissue regeneration and enhancing cell proliferation and adhesion.

* Corresponding author: hjz2002@xju.edu.cn
https://doi.org/10.15251/DJNB.2025.201.315

Hydroxyapatite (HA), a bioceramic coating, exhibits an apatite composition closely similar to that of bone tissue. In orthopedic applications, HA exhibits excellent biocompatibility and promotes osseointegration, thereby accelerating the generation of new osteoblasts. The large specific surface area of HA enhances cell adhesion and migration. Electrochemical deposition is a simple, cost-effective, and rapid method for preparing HA[3], enabling the formation of homogeneous coatings with dense and diverse morphologies on complex porous titanium structures. Used electrochemical to prepare HA and observed that variations in crystal growth morphology resulted from changes in crystal orientation at different stages of this process[4]. Developed a planar structure morphology by controlling HA growth orientation and found that this structure was less effective for cell proliferation[5]. Therefore, the morphology of the coating is a key factor in enhancing biological properties of the composite.In this study, sodium citrate was introduced into the electrolyte during electrochemical deposition to regulate HA morphology through the control of its grain growth orientation. Cellular experiments were performed to evaluate the impact of HA nanomorphology on biological properties to achieve the desired bioactivity in functionalized coated scaffolds.

2. Materials and methods

2.1. Bio-coating preparation

Porous scaffolds served as the cathode, while a platinum sheet was used as the anode during the electrochemical deposition process. The electrolyte comprised calcium nitrate tetrahydrate [$Ca(NO_3)_2 \cdot 4H_2O$] and ammonium hydrogen phosphate [$(NH_4)_2HPO_4$]. The pH of the electrolyte solution was adjusted to 4.2–4.4. Deposition was conducted at a constant current density of 4.5 mA/cm² and a temperature of 75°C for 90 min to prepare HA. Sodium citrate was incorporated into the electrolyte, and the samples prepared under the same conditions were denoted as CHA . Additionally, to prepare the T1, T2, and T3 samples, an electrolyte containing 6 wt% sodium citrate was used, with deposition times set at 60, 90, and 120 min, respectively. After preparation, all samples were immersed in 1 M NaOH for 2 h, rinsed with deionized water, and then dried in an oven at 37°C.

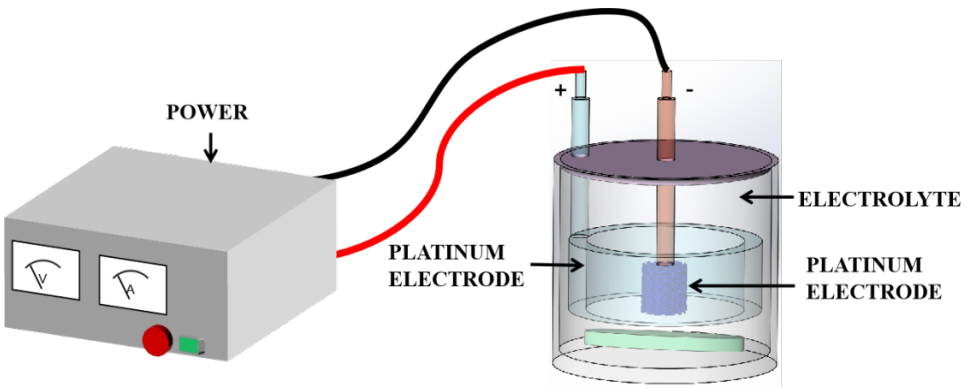

Fig. 1. Electrochemical deposition system.

2.2. In vitro studies

Cells were cultured in a complete medium composed of 89% α-MEM basal medium, 10% fetal bovine serum, and 1% penicillin-streptomycin. The cultures were maintained in a 5% CO_2 incubator at 35°C, with the medium replaced every 2 days. Bone marrow mesenchymal stem cells (BMSCs) were seeded onto the scaffolds at a density of 4×10^4 cells per scaffold and cultured for 7 days.At the end of the incubation period, the cells were fixed with 3% glutaraldehyde for 2 h. After fixation, the samples were washed three times with phosphate-buffered saline, with each wash lasting for 20 min. The samples were then sequentially dehydrated in 30%, 50%, 70%, 90%, and 100% anhydrous ethanol for 10 min each. Subsequently, the samples were placed in a freeze-dryer to remove residual water. After gold coating, the adhered cells on the coated surfaces were examined via SEM.Cell proliferation was assessed through the MTT assay. BMSCs were seeded onto the samples at a density of 3×10^4 cells per sample. After incubation periods of 1, 3, 5, and 7 days, 200 μL of a 5 mg/mL MTT solution was added to each sample and incubated at 37°C to facilitate the formation of insoluble formazan crystals. Subsequently, the MTT solution was removed, and the formazan crystals were dissolved in 1 mL of dimethyl sulfoxide. The optical density (OD) of the resulting solution was measured at 490 nm using a microplate reader.

2.3. Statistical analysis

The experimental data were presented as the mean ± standard deviation from four independent experiments. Statistical significance was assessed using analysis of variance and Student's t-test. A p-value of less than 0.05 was considered statistically significant.

3. Results and discussion

3.1. Effect of sodium citrate on HA morphology

SEM images reveal the morphology of HA crystals after the addition of sodium citrate to the electrolyte. Figures 2a–b show the morphology of citrate-modified HA. This modified coating material exhibits a needle-like fibrous structure. The grain growth orientation remains isotropic across the non-inhibited crystal surfaces. In contrast, HA formed without sodium citrate exhibits a needle-like structure characterized by a disordered surface growth (Figure 2d). A comparison of Figures 2b and e indicates that the addition of sodium citrate alters the densification of the coating. Without inhibition from citrate ions ($Hcit_2^-$), the gaps between crystals widen, and disordered growth increases the susceptibility of the crystals to agglomeration[6]. This behavior can be attributed to the rapid nucleation rate of grains exceeding their growth rate, leading to the aggregation of smaller crystals into spherical shapes. This suggests that the addition of sodium citrate alters the surface charge of HA crystals, thereby inhibiting crystal agglomeration[7]. Moreover, the EDS analysis of the surface morphology of the sodium citrate-modified coating revealed the presence of calcium and phosphorus, which were the main components of HA. The Ca/P ratio was 1.54, which was lower than the typical ratio of 1.65, suggesting that sodium citrate reacted with calcium ions to form calcium-deficient HA crystals.

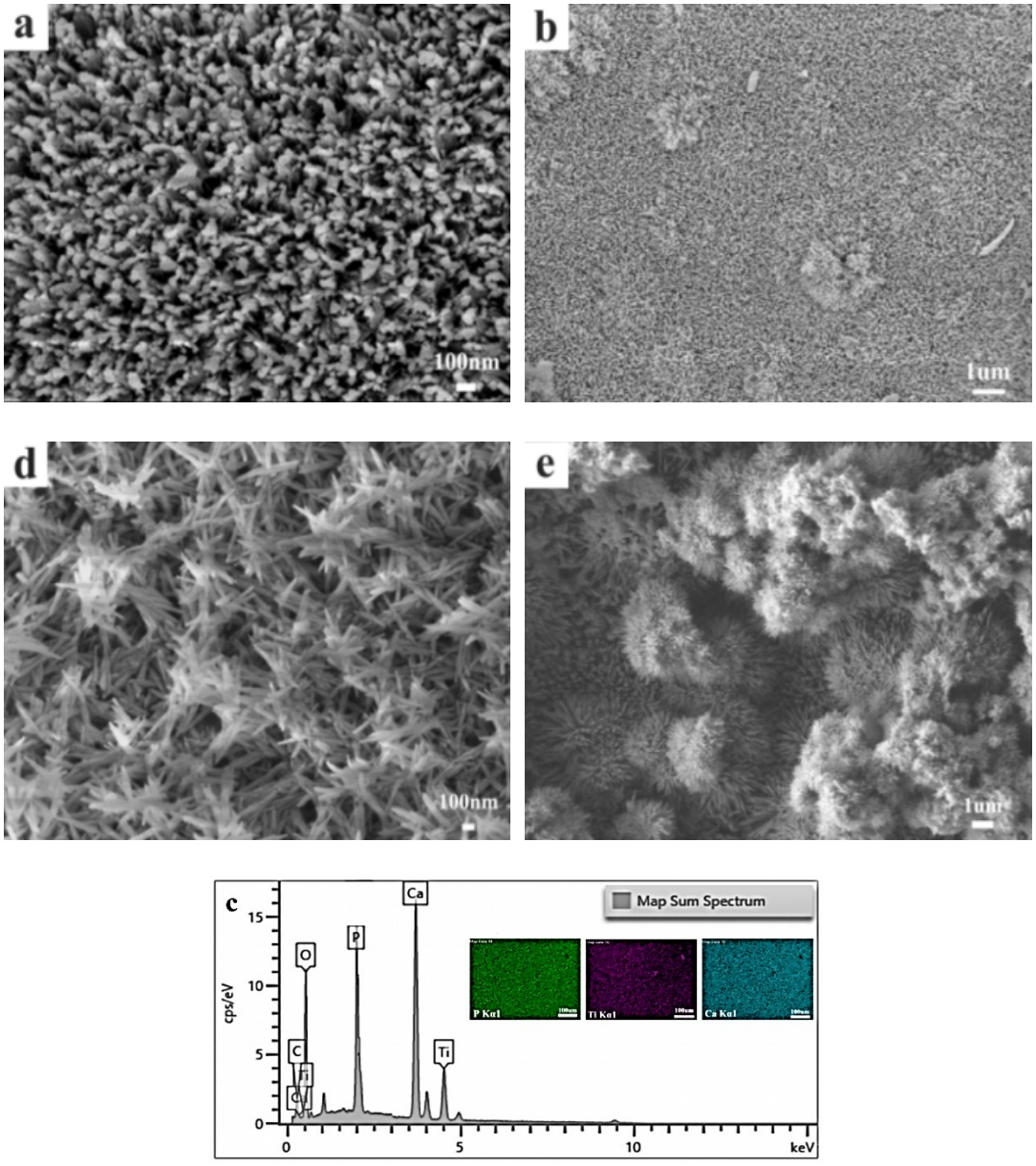

Fig. 2. (a, b) Surface morphology of HA(CHA) at low and high magnifications with the addition of sodium citrate. (c,d) Surface morphology of HA at low and high magnifications without sodium citrate. (e) EDS analysis of the surface elemental composition and Ca/P ratio in CHA.

Generally, HA forms a hexagonal crystal system composed of two principal planes: the a, b plane and the c plane. The c plane is mainly stabilized by negative charges, such as phosphate (PO_4^{3-}) and hydroxyl (OH^-) ions, while the a, b plane contains a higher concentration of positively charged calcium (Ca^{2+}) ions[8]. The distribution of anionic and cationic ions across the crystal planes contributes to the anisotropic behavior of HA crystals. The addition of sodium citrate results in the formation of $Hcit_2^-$, which causes the positively charged calcium ions on the a, b planes to preferentially attract free acid ions in the electrolyte[9]. This interaction inhibits the influence of other anions and promotes preferential HA crystal growth along the c plane.

Consequently, growth along the a and b planes is suppressed, resulting in the formation of needle-like or columnar HA morphologies oriented perpendicular to the substrate.

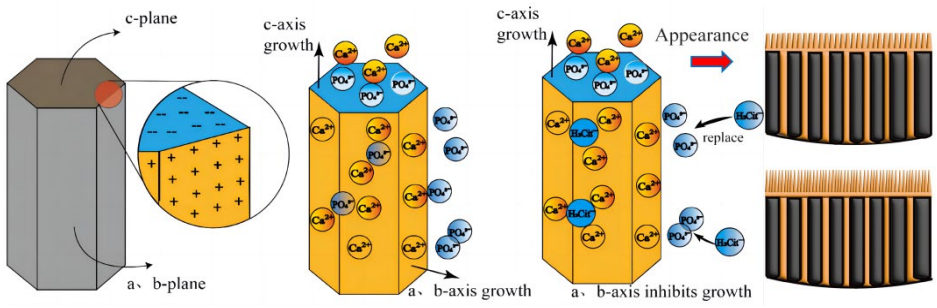

Fig. 3. Schematic illustrating the mechanism through which sodium citrate controls the orientation of HA crystal growth.

Figure 4 illustrates the effect of deposition time on HA morphology in the presence of sodium citrate. HA was deposited on porous substrates for 60, 90, and 120 min. The results revealed a strong correlation between coating morphology and deposition time. After 60 min, HA exhibited a short, needle-like structure. Sodium citrate inhibited HA grain growth along the a, b planes, promoting unidirectional growth along the c plane[10]. As the deposition time increased, HA grains continuously grew, leading to a significant consumption of $Hcit^{2-}$. However, the concentration of $Hcit^{2-}$ remained sufficient to suppress growth on the a, b planes. After 90 min, the HA crystals exhibited a pronounced needle-like HA structure, with an increase in both length and diameter (Figures 4c and d)[11]. After 120 min, the HA morphology transitioned to a plate-like structure. This change indicates that as $Hcit^{2-}$ was gradually consumed, its ability to inhibit growth along the a, b planes diminished. Consequently, the competition between $Hcit^{2-}$ and PO_4^{3-} decreased, leading to a reduced effectiveness of $Hcit^{2-}$ in suppressing growth along the a, b planes. This change results in a transition from ordered needle-like structures to plate-like shapes in the HA crystals.

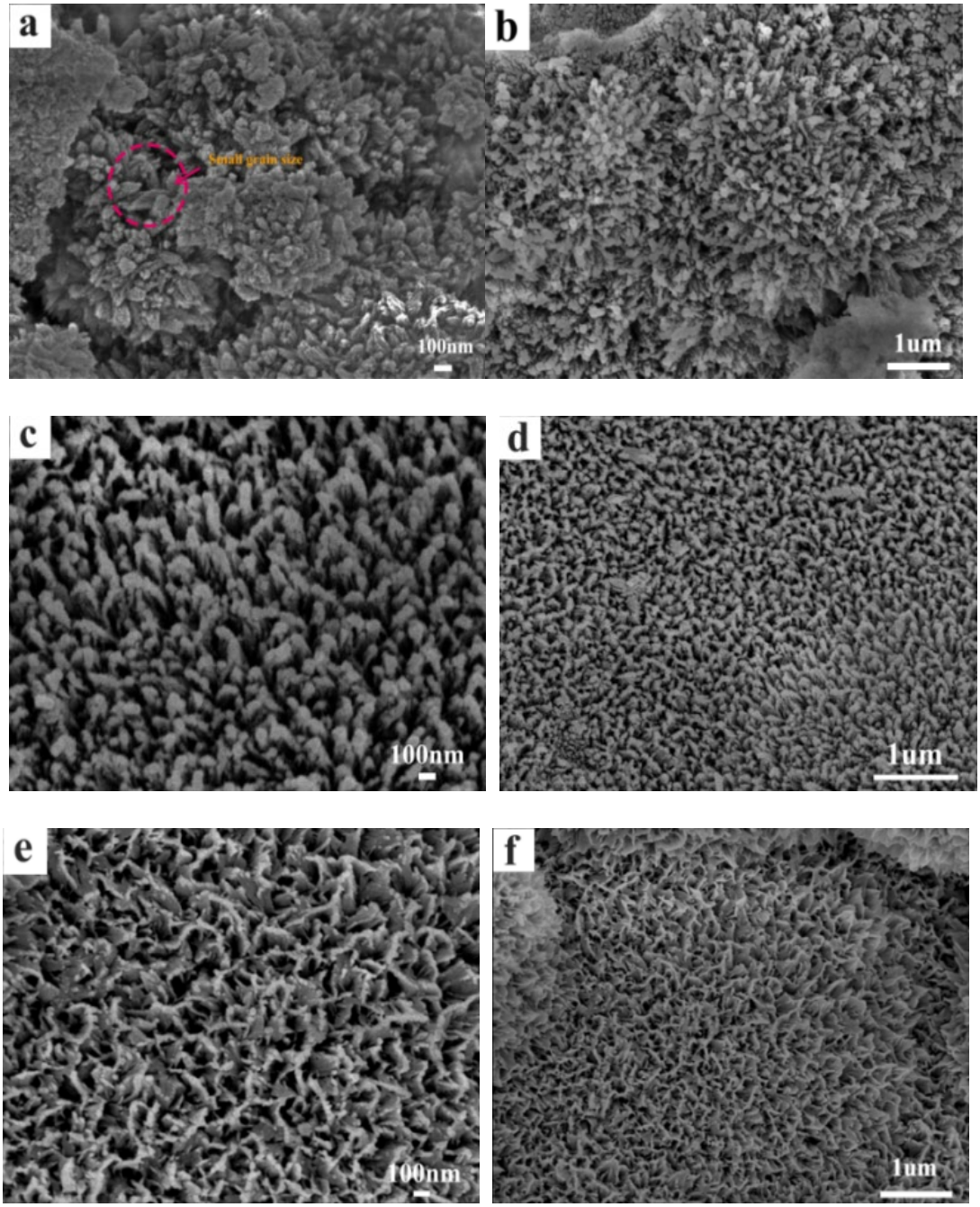

Fig. 4. SEM images of HA morphology at various deposition times with the addition of sodium citrate. (a) and (b) HA morphology at different magnifications after 60 min (T60). (c) and (d) HA morphology at different magnifications after 90 min (T90). (e) and (f) HA morphology at different magnifications after 120 min (T120).

3.2. Chemical analysis of coating surfaces

The effect of sodium citrate on the nucleation and growth of HA grains was assessed using the XRD spectra of samples prepared with and without sodium citrate. The XRD patterns revealed that all samples exhibited high-purity HA under the specified electrochemical deposition

conditions. A comparison of the XRD pattern with the PDF standard card confirmed that the characteristic diffraction peaks of the samples matched those of the standard card. Notably, the diffraction peaks corresponding to the (121) and (112) crystal planes of HA samples with sodium citrate exhibited varying intensities. Particularly, the intensity of the diffraction peak at the (002) crystal plane significantly increased, indicating that sodium citrate promoted the preferential growth of HA grains along the c-axis. HA grain morphology could be controlled through the addition of a specific concentration of sodium citrate. However, sodium citrate affected both the nucleation and growth rates of the crystals. The slower growth rate led to the formation of crystals with more regular structures[12] and fewer internal defects, such as dislocations and vacancies, thereby enhancing their ability to withstand stress.

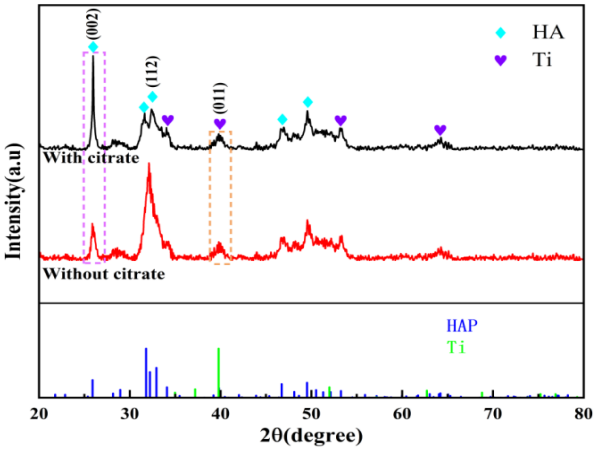

Fig. 5. XRD patterns of HA coatings prepared in different electrolytes.

FTIR analysis was performed to identify the chemical bonds in the HA coatings. Figure 6 presents the FTIR spectra of HA produced using different electrolyte compositions. The analysis of the functional groups corresponding to the primary peaks indicated that both samples, with and without sodium citrate, exhibited characteristic bands of HA. The peak at 3570 cm^{-1} corresponded to the stretching vibrational absorption of hydroxyl groups, while the peaks at 1035 cm^{-1} were associated with the stretching vibrational absorption of phosphate groups. The peaks at 604 and 566 cm^{-1} corresponded to the deformation vibrational absorption of phosphate[13]. A peak at 875 cm^{-1} can be attributed to the vibrational absorption of CO_3^{2-}, likely resulting from CO_2 uptake from the air during stirring and electrochemical reactions[14]. A comparison of the peaks across different spectral regions revealed that unlike HA without citric acid, the spectrum of HA with citric acid exhibited two absorption peaks at 1424 and 1480 cm^{-1}, corresponding to stretching vibrations of carboxylate groups. The intensity of the peaks at 1035 cm^{-1} associated with the phosphate stretching vibration decreased owing to the replacement of some phosphate ions by citrate ions, which bound to calcium ions.

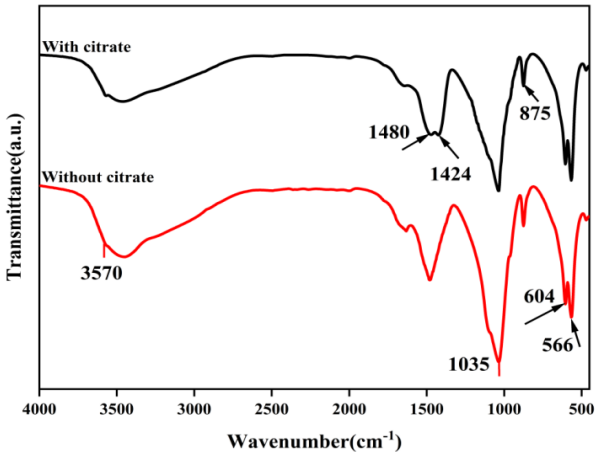

Fig. 6. FTIR spectra of HA coatings prepared without different electrolytes.

3.3. Biological activity

Light microscopy revealed that cell pseudopods displayed pronounced stretching morphology and adhered strongly to the Petri dish surface as the culture duration increased. SEM analysis was used to examine the adhesion and migration of cells on the different coating surfaces. Regardless of the sodium citrate addition, cells extended across the HA surfaces. On the HA surface modified with sodium citrate, cell pseudopods extended in various directions toward HA crystals, forming a polygonal morphology (Figure 7d). Additionally, these pseudopods integrated with loosely packed HA crystals, indicating that the modified HA morphology promoted cytoplasmic growth and improved cell-coating adhesion. In contrast, cells on the HA surface without sodium citrate exhibited limited diffusion (Figure 7c). This limited cell diffusion was due to the less compact arrangement of the HA crystals, which hindered the ability of cells to establish suitable adhesion points, thereby restricting pseudopod extension. Conversely, the coating with sodium citrate exhibited a more compact crystal morphology and lower porosity, which positively influenced cell adhesion and morphology[15,16].

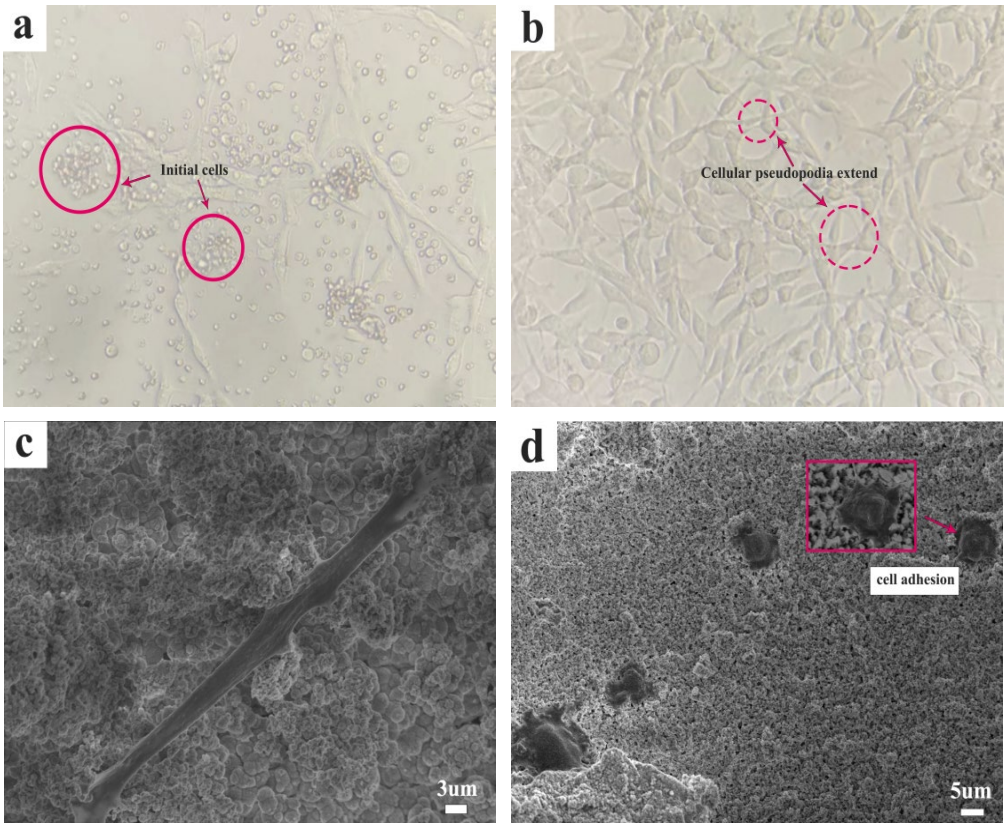

Fig. 7. Optical microscopy of cell morphology: (a) cell morphology after 3 days of culture; (b) cell morphology after 7 days of culture. SEM images of different TC4 samples cultured for 3 days: (c) HA-Ti cell morphology; (d) CHA-Ti cell morphology.

Cell proliferation on various samples was evaluated using the MTT assay, with OD values serving as indirect indicators of viable cell counts, according to Kozan's method. Cells were cultured on the samples for 1, 3, 5, and 7 days (Figure 8). BMSCs exhibited varying proliferation levels across all samples. After 1 day of culture, no significant differences in cell numbers were observed among the sample groups. By day 3, cell proliferation rates varied among the samples. Particularly, HA containing sodium citrate exhibited a higher number of cells than HA without sodium citrate. By day 5, cell proliferation levels remained similar to those observed on day 3. On day 7, cell proliferation continued. HA with added sodium citrate exhibited the highest cell count, with no significant difference compared to unmodified HA. Although HA morphology may influence cell migration and pseudopod extension, it did not significantly affect osteoblast proliferation. Moreover, sodium citrate reduced the growth rate of HA crystals but hindered their capacity to release reactive calcium and phosphorus ions, which are crucial for promoting cell proliferation and differentiation[17]. Furthermore, the Ca/P ratio in the crystals influenced cell proliferation, protein adsorption, and osteogenic differentiation[18]. The interaction between citrate ions and calcium ions led to a significant depletion of calcium, potentially forming HA with a lower Ca/P ratio. Compared with Ti, HA-coated surfaces facilitated a higher cell count. This suggests that HA can enhance the proliferation of BMSCs, thereby meeting the requirements for bone growth in implant applications.

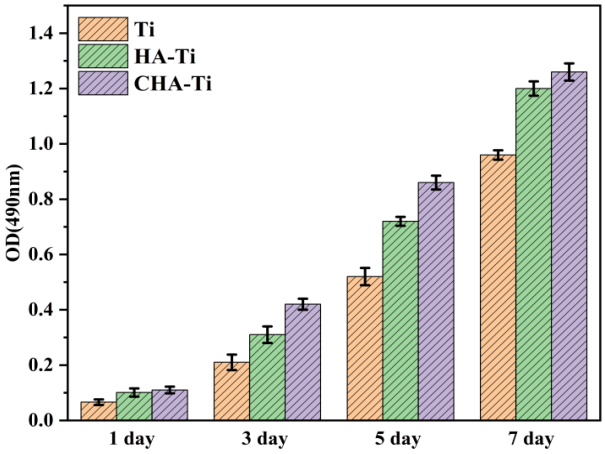

Fig. 8. MTT assay results of cells cultured on different TC4 samples for 1, 3, 5, and 7 days. All differences are statistically significant with $p < 0.05$.

4. Conclusion

In summary, HA with an optimal morphology were successfully synthesized on porous, curved titanium scaffolds via electrochemical deposition. Sodium citrate was introduced during HA synthesis. The incorporation of sodium citrate into HA significantly affected their morphology and bioactivity. Sodium citrate thereby facilitating grain growth along the c-axis, as confirmed by XRD and FTIR analyses, promoted the formation of needle-like and plate-like HA crystals. Moreover, biological assays revealed that both HA coatings significantly facilitated cell proliferation, with denser coatings promoting improving cell adhesion and spreading. These findings indicate the potential of sodium citrate to enhance the performance of HA-TNT coatings in biomedical applications.

Declaration of Conflicting Interests

The author(s) declared no potential conflicts of interest regarding the research, authorship, and/or publication of this article.

Acknowledgments

The author(s) acknowledge the financial support for the research, authorship, publication of this article from the National Natural Science Foundation of China (No.52165026) and the Open Subjects of the State Key Laboratory of Mechanical Manufacturing Systems Engineering, Xi'an Jiaotong University (No. sklms2021011).

References

[1] Aufa A, Hassan Z M, Ismail Z, et al., Journal of Materials Research and Technology,2024;31:213-243; https://doi.org/10.1016/j.jmrt.2024.06.041

[2] Zheng Y, Han Q, Wang J, et al., ACS Biomaterials Science & Engineering,2020;6(9):5181-5190; https://doi.org/10.1021/acsbiomaterials.0c00662

[3] Ling Y, Yi X, Jia Y, et al., ACS applied materials & interfaces,2017;9(5):5023-5030; https://doi.org/10.1021/acsami.6b15979

[4] Mokabber T, Lu L, Rijn V P, et al., Surface & Coatings Technology,2018;334:526-535; https://doi.org/10.1016/j.surfcoat.2017.12.011

[5] Zhuang Z, Fujimi J T, Nakamura M, et al., Acta Biomaterialia,2013;9(5):6732-6740; https://doi.org/10.1016/j.actbio.2013.02.001

[6]Kesarwani U, Basu B, Dubey K A, Applied Materials Today,2024;36:102062; https://doi.org/10.1016/j.apmt.2024.102062

[7] Jin X, Zhuang J, Zhang Z, et al., Journal of Colloid And Interface Science,2015;443:125-130; https://doi.org/10.1016/j.jcis.2014.12.010

[8] Priya Ranjan Dev, Chekkottu Parambil Anand, Materials Advances, 2022;3:7773-7809; https://doi.org/10.1039/D2MA00620K

[9] Ibrahim M, Labaki M, Giraudon J, et al., Journal Journal of Hazardous Materials,2020,383121139; https://doi.org/10.1016/j.jhazmat.2019.121139

[10] A M M, Catarina S, Margarida M A , et al., Journal of colloid and interface science,2008;318(2):210-216; https://doi.org/10.1016/j.jcis.2007.10.008

[11] Santos, Catarina,Almeida, et al., Crystal growth & design,2015;15(9):4417-4426; https://doi.org/10.1021/acs.cgd.5b00737

[12] Fernandes H M, Alves M M, Cebotarenco M, et al., Materials Science & Engineering C,2020;115(prepublish):111-147; https://doi.org/10.1016/j.msec.2020.111147

[13] Cotrut M C, Vladescu A, Dinu M, et al., Ceramics International,2018;44(1):669-677; https://doi.org/10.1016/j.ceramint.2017.09.227

[14] Chen J, Liu J, Deng H, et al., Ceramics International,2020;46(2):2185-2193; https://doi.org/10.1016/j.ceramint.2019.09.203

[15] Yulin L, Yin X, Changsheng L, reviews,2017;117(5):4376-4421; https://doi.org/10.1021/acs.chemrev.6b00654

[16] Amani H, Arzaghi H, Bayandori M, et al., Advanced Materials Interfaces,2019;6(13):1900572; https://doi.org/10.1002/admi.201900572

[17] Zhang L, Liang X, Chen J, et al., Ceramics International, 2024; 50(18PB), 33153-33163; https://doi.org/10.1016/j.ceramint.2024.06.126

[18] Luhui Z, Teliang L, Fupo H et al., Ceramics International,2022;48(17):24765-24776; https://doi.org/10.1016/j.ceramint.2022.05.126